Astronomy & Astrophysics manuscript no. Poly
June 22, 2009

Polytropic neutron star – black hole merger simulations with a Paczyński-Wiita potential

M. Ruffert[2,1] and H.-Th. Janka[1]

[1] Max-Planck-Institut für Astrophysik, Karl-Schwarzschild-Str. 1, D-85748 Garching bei München, Germany
e-mail: thj@mpa-garching.mpg.de
[2] The School of Mathematics and the Maxwell Institute, University of Edinburgh, King's Buildings, Edinburgh EH9 3JZ, U.K.
e-mail: m.ruffert@ed.ac.uk

Preprint online version: June 22, 2009

ABSTRACT

Context. Mergers of neutron stars (NS) and black holes (BH) are among the strongest sources of gravitational waves and are potential central engines for short gamma-ray bursts.
Aims. We aim to compare the general relativistic (GR) results by other groups with Newtonian calculations of models with equivalent parameters. We vary the mass ratios between NS and BH and the compactness of the NS. The mass of the NS is 1.4 $M_\odot$. We compare the dynamics in the parameter-space regions where the NS is expected to reach the innermost stable circular orbit (ISCO) before being tidally disrupted (mass shedding, MS), and vice versa.
Methods. The hydrodynamics is evolved by a Newtonian PPM scheme with four levels of nested grids. We use a polytropic EoS ($\Gamma = 2$), as was done in the GR simulations. However, instead of full GR we use a Newtonian potential supplemented by a Paczyński-Wiita-Artemova potential for the BH, both disregarding and including rotation of the BH.
Results. If the NS is compact ($C = 0.18$) it gets accreted by the BH more quickly, and only little mass remains outside the BH. If the mass ratio is small ($Q = 2$ or 3) or the NS is less compact ($C = 0.16$ or less) the NS gets tidally torn apart before being accreted. Although most mass gets absorbed by the BH, some 0.1 $M_\odot$ remain in a tidal arm. For small mass ratios ($Q = 2$ and 3) the tidal arm can wrap around the BH to form a thick disk. When including the effects of BH spin-up or spin-down by the accreted matter, more mass remains in the surroundings (0.2–0.3 $M_\odot$).
Conclusions. Although details and quantitative results differ, the general trends of our Newtonian calculations are similar to the GR calculations. A clear delimiting line that separates ISCO from the MS cases is not found. Inclusion of BH rotation as well as sufficient numerical resolution are extremely important.

Key words. Hydrodynamics – Black Hole Physics – Methods: numerical – Binaries:close – Stars:neutron

1. Introduction

Merging binaries of neutron stars (NS) and black holes (BH) are of interest both as possible central engines for short gamma-ray bursts and as promising gravitational wave sources detectable by the interferometer observatories. As computational power and numerical schemes have progressed so has the detail of simulations of such mergers. Early simulations by our group (Janka et al. 1999) were aimed toward investigating gamma-ray burst scenarios. We had included detailed microphysics (equation of state, neutrino source terms) but had accounted for general relativistic effects only partially (gravitational wave emission and backreaction) or phenomenologically (Paczyński-Wiita potential for the BH). Other groups interested in the gravitational wave aspects have recently published results of NS–BH mergers with general relativistic (GR) physics (Etienne et al. 2009, Shibata et al. 2009, Rantsiou at al. 2008, Taniguchi et al. 2008), but with some variant of polytropic equation-of-state (EoS) for the neutron star matter.

We would like to compare the results of a partially post-Newtonian calculation of NS–BH mergers with the published GR simulations, in particular to address the following aspect: Miller (2005) and Taniguchi et al. (2008) pointed out that during the NS–BH binary orbital inspiral, the innermost stable circular orbit (ISCO) can be reached before the NS gets tidally disrupted. In this case it is to be expected that most of the NS matter is swallowed by the BH before the material can spread out and form a massive torus. Since the ISCO is a purely general relativistic effect, its consequences will not be seen in a purely Newtonian simulation. However, the Paczyński-Wiita potential (Paczyński & Wiita 1980, Abramowicz 2009) phenomenologically mimics the ISCO in a Newtonian setting. So the question arises whether and to what extent one can reproduce the results of the general relativistic simulations with crude Newtonian approximations.

Which of the two cases — NS reaches ISCO first or NS gets tidally disrupted first — happens during the evolution will have a direct impact upon the amount of mass remaining in the torus around the BH. This mass is supposed to provide the energy for the jet of the short-duration gamma-ray bursts, so less mass implies a dimmer burst. Intrinsically, the tidal disruption — called 'mass shedding' (MS) in previous papers — should yield a more massive torus than the ISCO case. As shown in our previous investigations (Ruffert et al. 2001 and references therein, Setiawan et al. 2006) fairly massive tori of a at least several hundredths of a solar mass seem to be needed for the scenario of a hot neutrino-emitting disk to function as central engine for gamma-ray bursts (Lee et al. 2005, Oechslin & Janka 2006). Thus the question of how the NS gets tidally disrupted or swallowed by the BH, and how much mass remains in the torus is an important one to explain gamma-ray bursts that needs to be investigated in detail.

Table 1. Key initial model parameters and some results. Initial parameters: mass ratio Q, compactness C, black hole mass $M_{\rm BH}$, neutron star radius $R_{\rm NS}$, initial orbital distance $d_{\rm i}$, size of largest grid L, size of finest zone $\Delta x = L/2048$. The mass of the NS is $1.4\,M_\odot$ in all cases. Values at the end of the simulation, only for high-resolution models: unbound+ejected gas mass $M_{\rm u}$, bound neutron star mass around BH $M_{\rm b}$, neutron star mass not instantly accreted by BH $M_{\rm g}$, |h/l| states whether the difference between values for $M_{\rm g}$ in low-resolution and high-resolution simulations is less than 20% (Yes/No; '-' no low-res model computed). The spin-up of the BH by accretion of matter is not taken into account.

Model	Q	C	$M_{\rm BH}$	$R_{\rm NS}$	$d_{\rm i}$	L	Δx	$M_{\rm u}$	$M_{\rm b}$	$M_{\rm g}$	|h/l|
			$M_\odot$	km	km	km	km	$M_\odot$	$M_\odot$	$M_\odot$	
M5.145	5	0.145	7.0	14.3	92	1550	0.77	0.07	0.08	0.15	N
M4.145	4	0.145	5.6	14.3	80	1400	0.68	0.08	0.10	0.18	Y
M3.145	3	0.145	4.2	14.3	68	1100	0.54	0.06	0.09	0.15	Y
M2.145	2	0.145	2.8	14.3	56	880	0.43	$< 10^{-2}$	0.07	0.08	Y
M5.160	5	0.160	7.0	12.9	92	1550	0.77	0.01	0.05	0.06	-
M4.160	4	0.160	5.6	12.9	76	1250	0.61	0.03	0.06	0.09	N
M3.160	3	0.160	4.2	12.9	66	1100	0.54	0.03	0.06	0.09	N
M2.160	2	0.160	2.8	12.9	52	820	0.40	$< 10^{-2}$	0.04	0.05	Y
M5.180	5	0.180	7.0	11.5	88	1500	0.73	$< 10^{-3}$	$< 10^{-3}$	$< 10^{-3}$	N
M4.180	4	0.180	5.6	11.5	76	1250	0.61	$< 10^{-3}$	$< 10^{-3}$	$< 10^{-3}$	N
M3.180	3	0.180	4.2	11.5	64	1050	0.51	$< 10^{-2}$	0.01	0.01	N
M2.180	2	0.180	2.8	11.5	50	780	0.38	$< 10^{-3}$	0.004	0.004	N

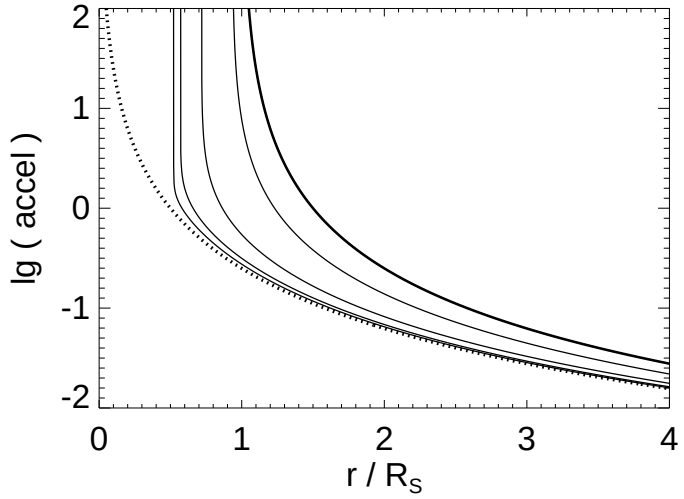

Fig. 1. Gravitational acceleration as function of distance r, as given by prescription Eq. (1), for various spin parameters a = 0.999, 0.99, 0.9, 0.5, 0; solid lines from left to right. The dotted line shows a Newtonian potential acceleration $\propto r^{-2}$. The bold solid line shows the Paczyński-Wiita case $\propto (r - R_{\rm S})^{-2}$, i.e. $a = 0$. $R_{\rm S}$ is the Schwarzschild radius.

The results of the currently published GR simulations still disagree with each other in this point.

Following the introduction above, this paper will describe the methods in the next section and results of the simulations in Section 3. These results are then discussed (Sect. 4) and the paper concludes with a summary (Sect. 5).

2. Methods

2.1. Theory and Numerical Formulation

The three-dimensional hydrodynamic simulations were performed with a basically Newtonian code based on the Piecewise Parabolic Method (PPM) of Colella & Woodward (1984) with four levels of nested grids (Ruffert 1992). The equidistant Cartesian grids all have the same number of zones, depending on the model, either 128 or 256 zones per dimension. Initially the finest grid covers both components of the system (neutron star and black hole). We use an ideal gas equation-of-state (EoS, $P = (\Gamma - 1)\epsilon$ with adiabatic index $\Gamma = 2$, pressure P and internal energy density ϵ) to close the energy equation evolved in the hydrodynamics code. The self-gravity of the gaseous mass distribution on the grids are calculated by fast-Fourier transforms (FFT).

The black hole (BH) of mass $M_{\rm BH}$ is treated as a gravitational point mass surrounded by a vacuum sphere discretised on the grids. The existence of the innermost stable circular orbit (ISCO) is mimicked by having a Paczyński-Wiita-type potential (Paczyński & Wiita 1980, Artemova et al. 1996). The Artemova et al. prescription for the acceleration is

$$\frac{{\rm d}\Phi_{\rm BH}}{{\rm d}r} = -\frac{GM_{\rm BH}}{r^{2-\beta}(r - r_{\rm H})^{\beta}}\,, \qquad (1)$$

where $r_{\rm H}$ is the black hole event horizon, and β is a constant for a given value of the BH spin parameter a. It is defined by $\beta(a) = (r_{\rm in}(a) - r_{\rm H}(a))/r_{\rm H}(a)$. Here $r_{\rm in}(a)$ is the radius of the ISCO. This prescription reduces to the usual Paczyński-Wiita potential when the BH spin parameter a is zero, then $\beta = 2$, and $r_{\rm H}(a = 0) = 2GM_{\rm BH}/c^2$. Note a mathematical discontinuity: for $\beta > 0$, $r_{\rm H}$ remains a lower limit for $r > r_{\rm H}$, whereas for $\beta = 0$ one recovers the Newtonian case for all $r > 0$ (see Fig. 1). The graphs of $r_{\rm H}(a)$, $\beta(a)$ and $r_{\rm in}(a)$ can be found in Setiawan et al. (2006), Fig. 1.

Technically numerically this potential is implemented as follows. First the total Newtonian potential is calculated for all gas on the grids and including the BH mass. From this potential the accelerations are derived by discrete differencing, as is common procedure. We then add the acceleration given by the difference between the formalism Eq. (1) and a purely Newtonian potential. By construction, this difference only acts on the gaseous NS matter on the grid. To respect Newton's Third Law ("action=reaction"), a tab of the sum of these accelerations has to be kept and its inverse enforced on the BH.

The radius of the vacuum sphere mimicking the BH is chosen to be the arithmetic mean of the event horizon and ISCO. Mass, momentum and angular momentum of material that flows across this inner boundary are added to the BH values and the zones affected reset to near-vacuum values. The position of the

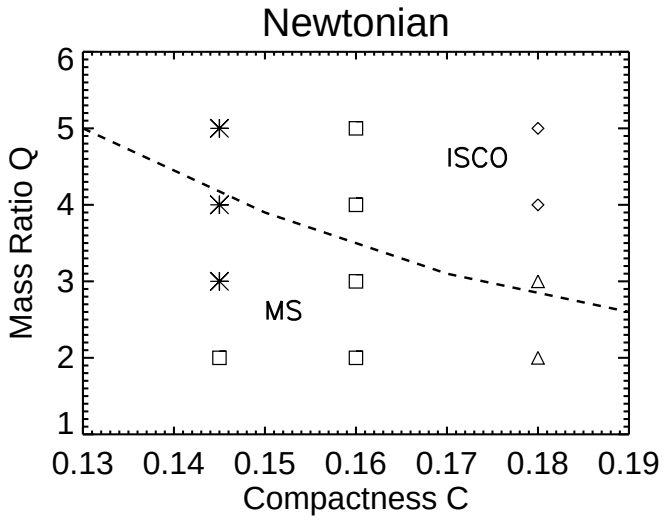

Fig. 2. Parameter space of models presented in this paper (only non-spinning BH), with compactness $C = (GM_{\rm NS})/(c^2R_{\rm NS})$ and mass ratio $Q = M_{\rm BH}/M_{\rm NS}$. Each symbol represents one model: 'diamond' $M_{\rm g} < 10^{-3}M_\odot$, 'triangle' $10^{-3}M_\odot < M_{\rm g} < 0.02M_\odot$, 'square' $0.02M_\odot < M_{\rm g} < 0.1M_\odot$, 'star' $0.1M_\odot < M_{\rm g}$, for the mass $M_{\rm g}$ not instantly accreted by the BH. Note that the spin-up of the BH by the accretion of matter is not take into account. The line separating innermost stable circular orbit (ISCO) and mass shedding (MS) regions is taken from Taniguchi et al. (2008).

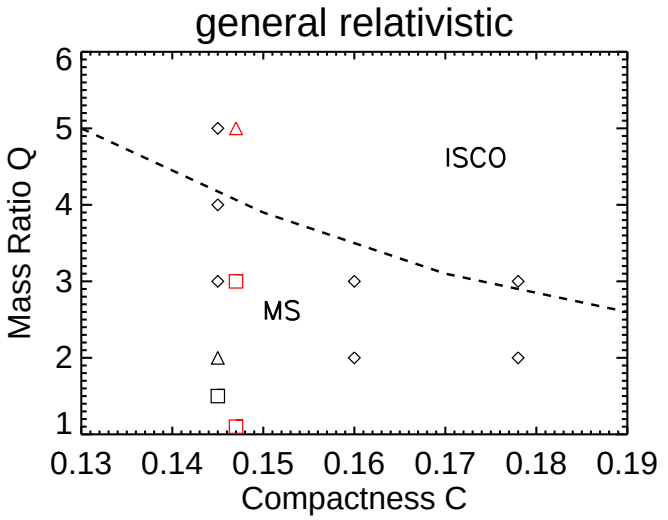

Fig. 3. Results of Shibata et al. (2009) and Etienne et al. (2009) (only non-spinning BH) models, with compactness C and mass ratio Q. Each symbol represents one model; the same symbols are used as in Fig. 2. The symbols for the Etienne et al. (2009) models are slightly shifted to $C = 0.147$ (and coloured red), for clarity.

BH is adjusted accordingly — the centre-of-mass of the gas taken off the grid and of the BH do not necessarily coincide — and moved by a leapfrog procedure (alternate position and velocity updates). In all models listed in Table 1, the angular momentum of the accreted material does not change the spin parameter a in the equations that determine the BH potential, Eq. (1); i.e. the BH potential only deepens through the increase in mass of the BH. We evolved an additional set of four models to investigate the effects of BH spin. These models are listed in Table 2 and are discussed in separate paragraphs.

The general relativistic effect being modeled phenomenologically by the procedures described above is the presence of the ISCO and its change in radius. Frame-dragging and many other effects, e.g. relativistic kinematics, redshift, time dilation, etc., are omitted. However we do include the local effects of gravitational-wave emission — the volume integral of which reproduces the quadrupole approximation — and the corresponding back-reaction on the hydrodynamic flow (for details see Ruffert et al. 1996).

2.2. Initial Conditions

The initial distance of NS to BH varies from model to model, to ensure roughly 2–3 orbits before coalescence (see Table 1). For the finest grid to cover both components of the binary, the geometric extent of the grids has to be adapted to ensure the highest possible numerical resolution. Both the extent of the largest grid as well as the size of the finest zone are listed in Table 1.

Parameters for the NS model are fixed as follows. The mass is kept constant for all polytropic models, $M_{\rm NS} = 1.4M_\odot$. The radius, $R_{\rm NS}$, follows from the chosen compactness, $C = (GM_{\rm NS})/(c^2R_{\rm NS})$. For a $\Gamma = 2$ polytrope the relation between pressure P and density ρ is $P = \kappa\rho^2$, with $\kappa = \frac{2}{\pi}GR_{\rm NS}^2$ fixed by the NS radius. The density distribution is $\rho(\xi) = \rho_c \frac{\sin(\xi)}{\xi}$, with $M_{\rm NS} = \frac{4}{\pi}R_{\rm NS}^3\rho_c$, and $\xi = \pi r/R_{\rm NS}$.

The main variable of the BH, its mass, is given by definition of the mass ratio with respect to the NS, $Q = M_{\rm BH}/M_{\rm NS}$. Both the NS and BH are initially given Keplerian velocities plus a small radial velocity component from the quadrupole approximation of gravitational wave emission.

In our Newtonian framework, there is no ambiguity concerning which masses and radii to use in the equations above. This is different from relativistic calculations, where a choice of masses (ADM, rest, etc.), and distances (isotropic, circumferential, etc.) exists. We will have to return to this point when trying to compare our results with other people's simulations, in Sect. 4.

When the NS is evolved in the simulation, the initially spherical NS adapts to the BH potential, orbital motion and grid resolution on its (NS) dynamical time scale, i.e. within much less than one orbital revolution. This initial phase is well over by the time the NS crosses the ISCO or gets tidally disrupted.

The actual values of the mass ratio Q and compactness C can be found in Table 1. They are also shown in Fig. 2 and were chosen to match closely the models presented in Shibata et al. (2009), see Fig. 3. Figures. 2 and 3 include the line separating the regions within which the NS first reaches the innermost stable circular orbit (ISCO) and the mass shedding limit (MS), respectively. It is taken from Taniguchi et al. (2008) and is based on quasi-equilibrium configurations of the binary system.

3. Results

3.1. Resolution and Convergence

Figure. 4 shows some results for both high-resolution as well as lower-resolution models. Simulations with smaller mass ratios and less compact NSs are intrinsically better resolved (see Table 1). The dynamics for these models and the results, e.g. gas mass on the grid after merger, match reasonably well for the high- and low-resolution calculations. Thus 128^3 runs, which are

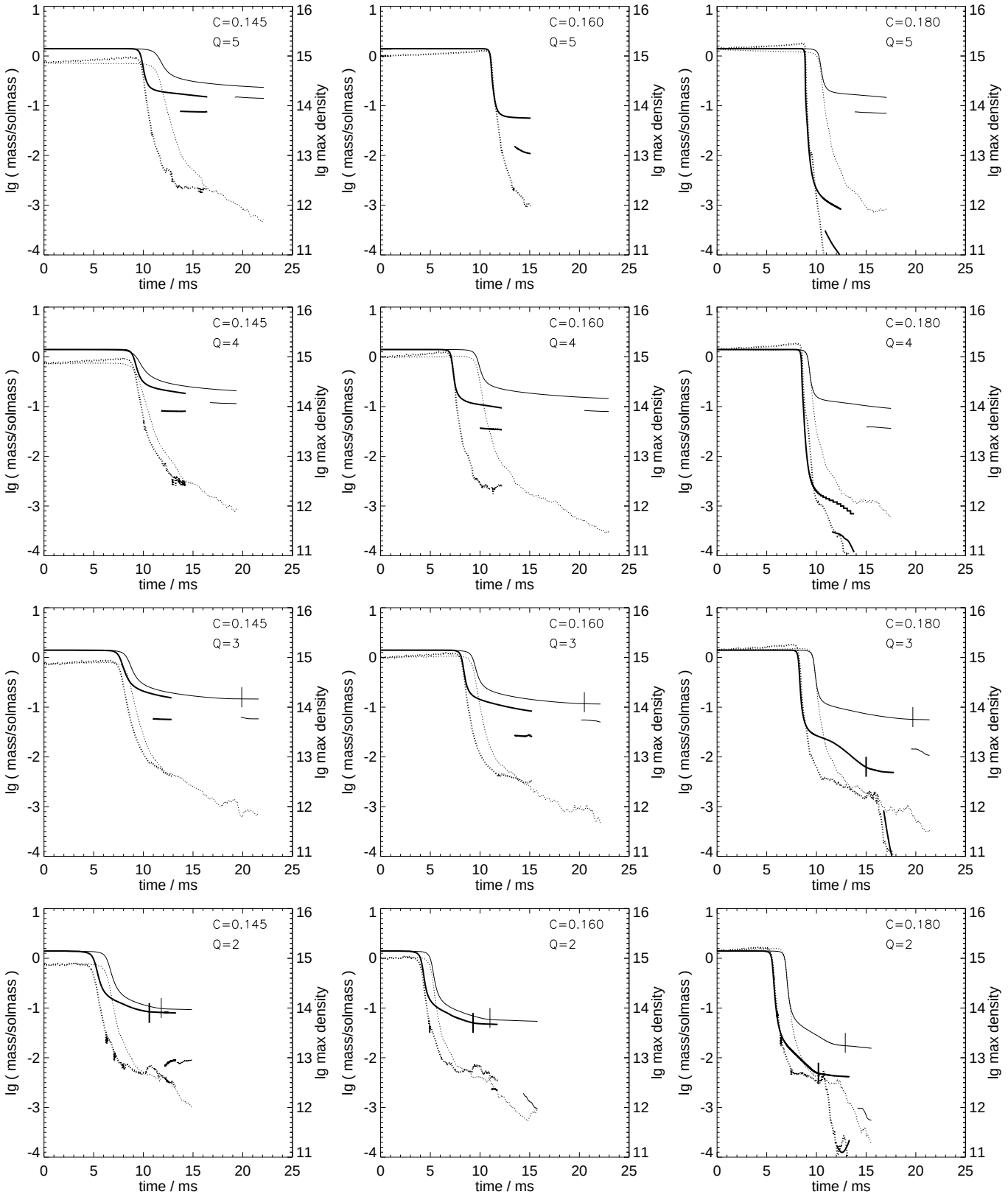

Fig. 4. Temporal evolution of some quantities for various models; the parameter values for Q and C are given within each panel. Solid lines show the gas mass. Dotted lines show the maximum density. Thin lines show lower-resolution simulations (128^3); bold lines show higher-resolution simulations (256^3). A short vertical line indicates the formation of an accretion disk. Short pieces of nearly horizontal lines show the amount of unbound mass.

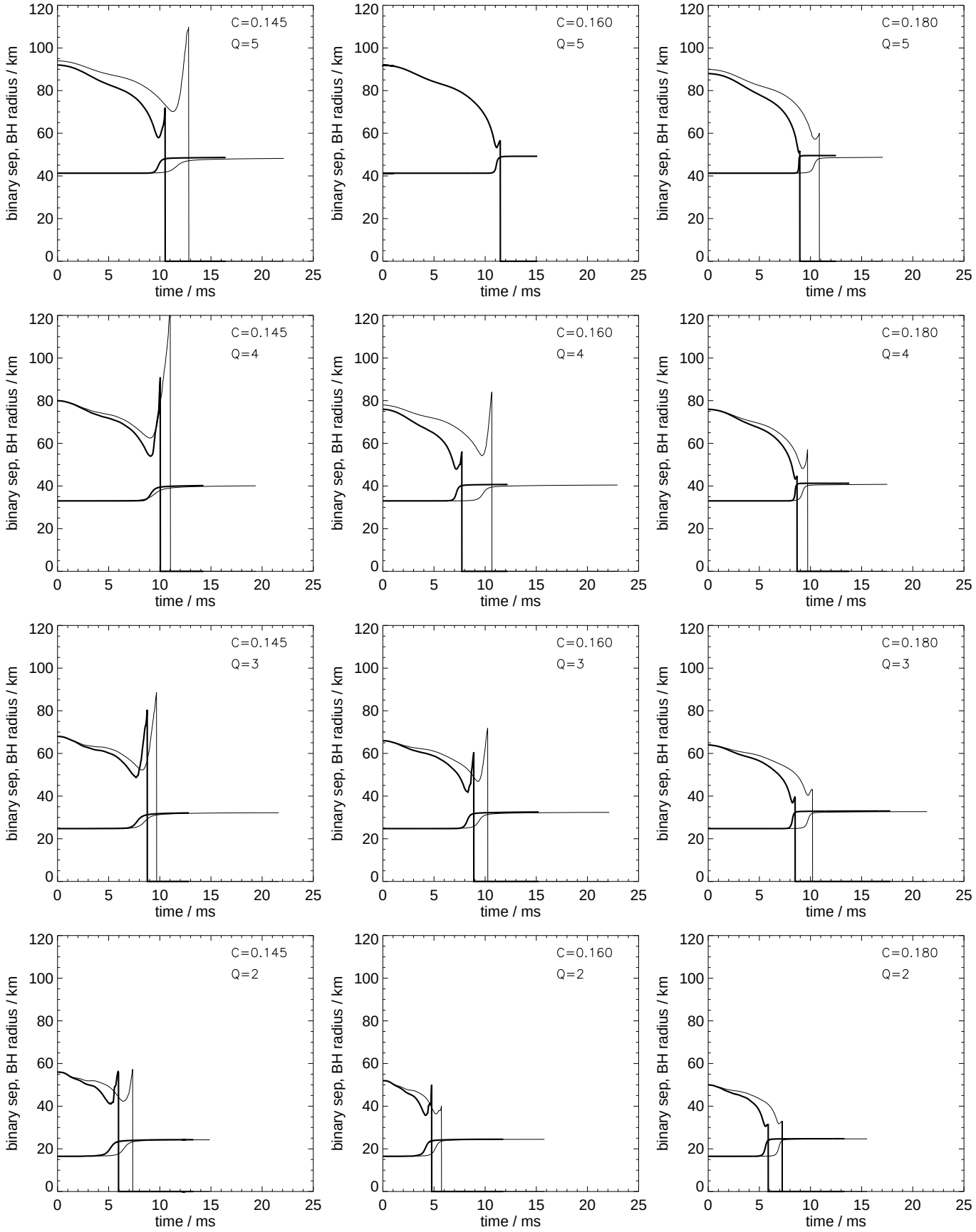

Fig. 5. Temporal evolution of some quantities for various models; the parameter values for Q and C are given within each panel. The upper pair of lines show binary separation; the lower pair of lines show radius of the BH (details see text). Thin lines show lower-resolution simulations (128^3); bold lines show higher-resolution simulations (256^3). The vertical line indicates when the mass within a sphere around the density maximum falls below 0.03 $M_\odot$.

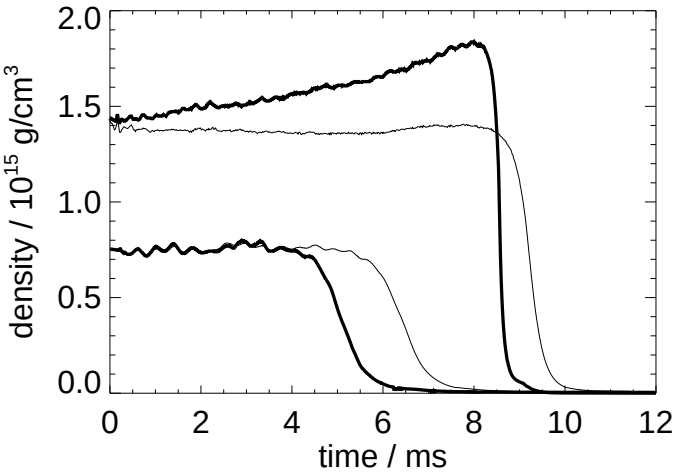

Fig. 6. Maximum density as function of time for two selected models. The upper pair of lines shows model M4.180; the lower pair of lines shows model M2.145. Thin lines show lower-resolution simulations (128^3); bold lines show higher-resolution simulations (256^3).

computationally feasible in a few days, yield converged results. However, the models with very compact NSs – which have comparatively fewer zones to cover the NS volume and in particular the steep surface gradients – or models with a large mass ratio – i.e. a large BH which in turn implies large zones – need at least 256^3 zones to be adequately resolved. This can also be seen in Fig. 6, for example: For model M2.145, both the low- and high-resolution simulations can hold the NS intact on the grid and thus the maximum density during the first few orbits are equal. On the other hand, the maximum density of the NS in model M4.180 is distinctly lower in the low-resolution simulation than in the high-resolution calculation, which indicates that the NS develops a more compact core during the initial orbital motion. For very low resolution models, the NS core actually dissolves secularly. The results of the low-resolution simulation for this model should be treated with caution. We have no reason to believe that the high-resolution simulations are compromised in this way, but are not able to perform even higher-resolution calculations to check this point.

3.2. Dynamical Evolution

We will describe the merger for the two most extreme cases (non-spinning BH) in our set of models: (1) A small BH with large NS, specifically a mass ratio of $Q = 2$ and a small value for compactness of $C = 0.145$. (2) A large BH with a small NS, specifically a mass ratio $Q = 5$ and a value for compactness of $C = 0.180$. These two models cover the main features seen in the simulations, while other models with intermediate values for Q and C are easily recognized as being similar to one or the other of the two cases.

3.2.1. Low mass ratio, small compactness

During the initial orbital decay of Model **M2.145** the central density of the NS remains fairly constant (Figs. 6 and 4). One notices small oscillations coming from the initially spherical NS adapting to the potential of the BH and the discretisation on the grid. At about 5 ms the closest distance of the NS density maximum or centre-of-mass is reached (Fig. 5 bottom left; Fig. 7 top left). Matter is being transferred to the BH at this point, but at a relatively (to the other case) slow rate. The NS is tidally disrupted, but not before a substantial portion of its matter is given an elliptic orbit taking it temporarily away from the BH: note the increase in distance of the density maximum in all cases of small mass ratio and small compactness (models on the lower and left hand side in Fig. 5). We will return to this point of orbital widening in Sect. 4.1. The "radius of the BH" shown in Fig. 5 is the arithmetic mean of the event horizon and innermost stable circular orbit, as described in Sect. 2.2. For a non-rotating BH this is equal to two Schwarzschild radii.

The NS matter spreads out in a tidal spiral arc containing $0.08\,M_\odot$ (Fig. 7 central left panel $t = 9.96$ ms). Eventually matter falls back along the spiral arc toward the BH. Some of it manages a full circle around the BH and then collides into the incoming material. At this point the infalling matter is deflected away from the BH, the circling material spreads out to fill space and a torus is formed. The point in time when this deflection happens is marked by a short vertical line in Fig. 4, and one can see that this applies only to models with small mass ratios $Q = 2$ and $Q = 3$, for all three compactnesses. In some cases the high-resolution models were not evolved long enough to see the formation of a disk.

A fraction of the material in the spiral arc is unbound. This amount is also indicated in Fig. 4, by a short piece of near-horizontal line. The values are listed in Table 1.

3.2.2. High mass ratio, large compactness

During the initial orbital decay of model **M5.180** the central density increases substantially (Fig. 6, similarly to model M4.180) in the calculations with sufficiently high resolution. This increase can be noted for all models with massive BHs, i.e. high mass ratios (close inspection of Fig. 4). So when the NS is close enough to finally transfer mass to the BH, it is very compact and mass transfer proceeds relatively quickly: note the very steep decline of the mass on the grid for this model M5.180, in contrast to M2.145 described above. Partially this effect is also due to the fact that for large BHs an increase of mass and radius will produce an essentially direct approach to the absorbing surface.

The distance of the NS's density maximum from the BH decreases continuously all the way down to the numerical surface of the BH. In the right panels of Fig. 5 one sees the line of separation nearly meet the line of BH radius to within a few km. The minimal distance shown in the opposite case of model M2.145 is much larger, approximately 15 km.

The NS matter remaining in model M5.180 after the merger, also spreads out in a tidal spiral arc, but it contains only $10^{-3}\,M_\odot$ (Fig. 4 and Fig. 8). The BH, having a very large extent, accretes all the material that flows back along the arc; none manages to flow all the way around the BH and form a disk.

Eventually the matter in the outermost portions of the spiral arc reaches the edge of largest grid (only the lower resolution simultations can be evolved for this length of time). For most models this happens at around 15-20 ms (depending on the model) at which point the amount of unbound matter ejected from the system is registered by the calculation. The amounts of matter ejected are approximately 10^{-3}–$10^{-2}\,M_\odot$. We also calculate the amount of material on the grid that is not gravitationally bound, by comparing the internal and kinetic energies to the potential. The values of these mass components are listed in Table 1 and are consistent with the amounts that actually flow off the coarsest grid as described above. Dividing the distance traveled by

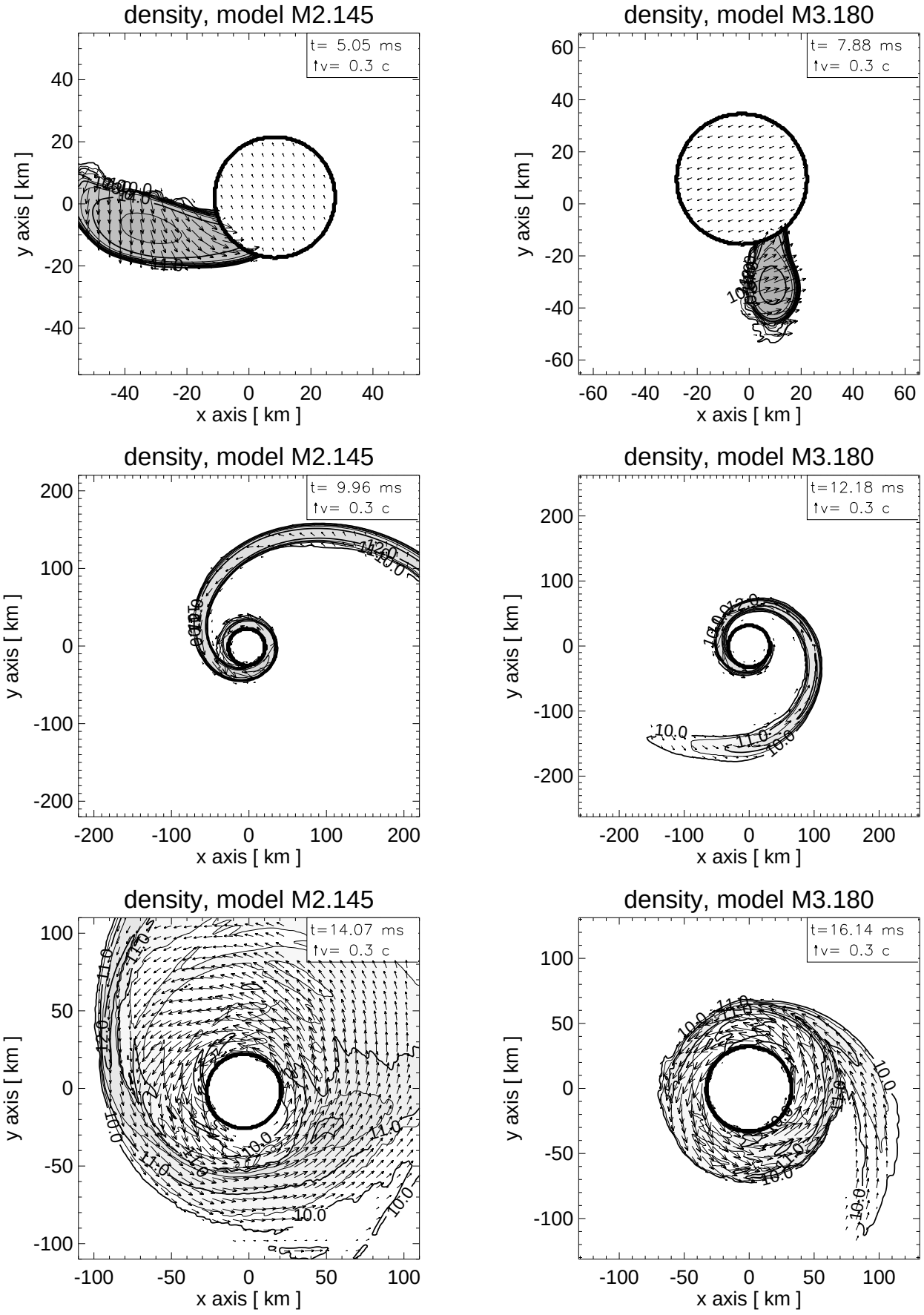

Fig. 7. The mass density distributions for models M2.145 and M3.180 are displayed in the orbital plane with contours spaced logarithmically in steps of 0.5 dex, with units g cm^{-3}. The arrows indicate the velocity field. The circle at the centre outlines the BH radius which is the arithmetic mean of the event horizon and ISCO.

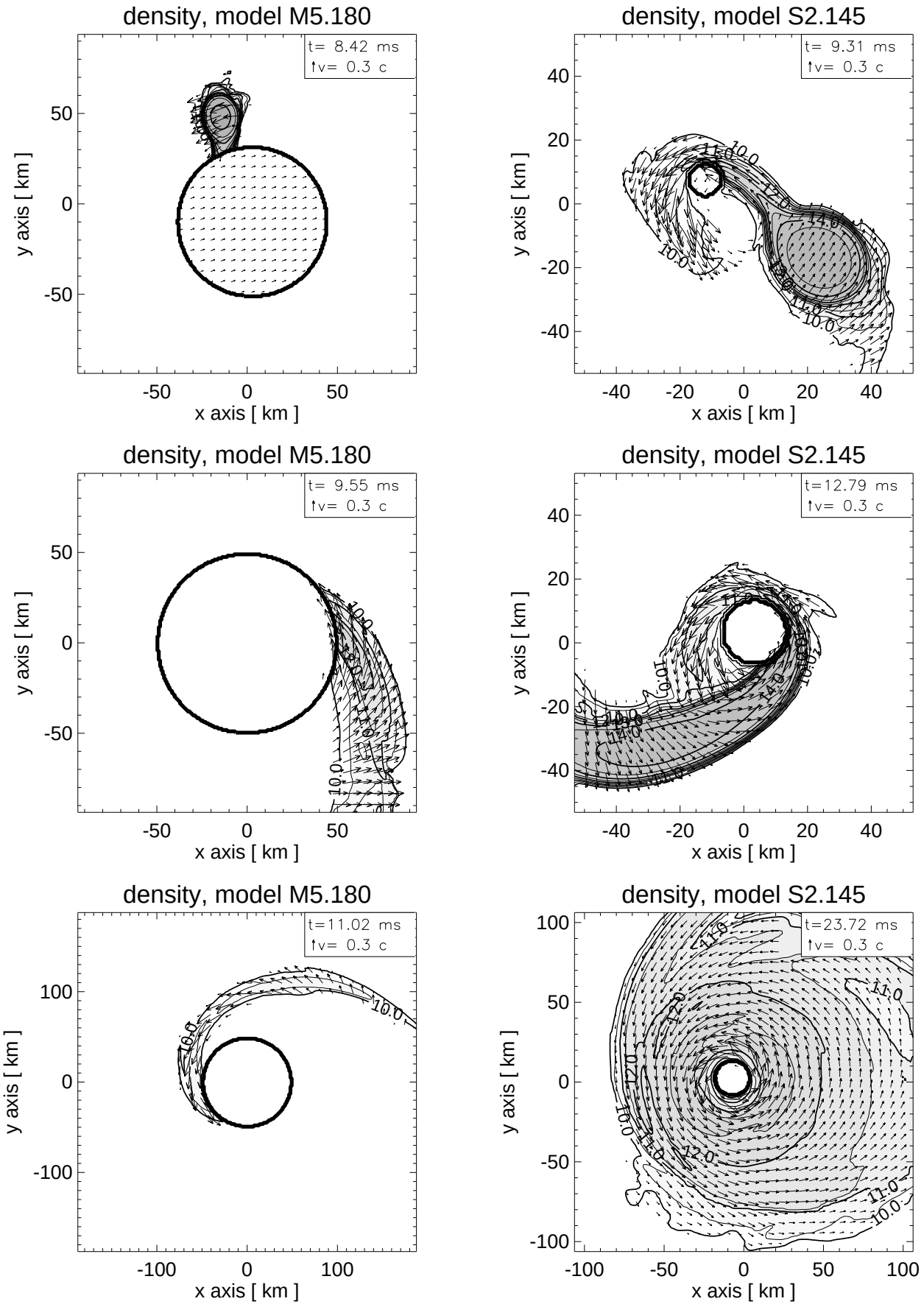

Fig. 8. The mass density distributions for models M5.180 and S2.145 are displayed in the orbital plane with contours spaced logarithmically in steps of 0.5 dex, with units g cm^{-3}. The arrows indicate the velocity field. The circle at the centre outlines the BH radius which is the arithmetic mean of the event horizon and ISCO.

this material – roughly half the grid size $L/2 \approx 400$ km – by the time elapsed between merger and arriving at the edge of the grid (approximately 5 ms), yields an average speed of c/4.

3.2.3. Comparison of models

Looking at Figs. 4 and 5 one sees that all models with $C = 0.145$ and $C = 0.160$ follow the patterns described above for model **M2.145**. All models with $C = 0.180$ follow the mass accretion pattern of **M5.180**, although some aspects of models M2.180 and M3.180 are different: the BH is small enough in these two cases to allow formation of a disk, albeit with a very small mass. We included the information on the mass remaining on the grids in Fig. 2 in an attempt to outline the similarities between the various models.

3.3. Effects of BH spin

We calculated four models to assess the influence of BH spin: in three models (R2.145, R3.160, R5.180) the BH is taken to be initially non-rotating ($a_\mathrm{i} = 0$), but we allowed a change of the BH potential due to spin-up by accretion of angular momentum of the NS matter during the evolution. The opposite case, an initially rapidly spinning BH with $a_\mathrm{i} = 0.99$, is simulated in model S2.145, and like the other three models, the spin and potential are allowed to change by accretion as well. The complete investigation of the effects of these changes is outwith the remit of this paper and is left to future work. Here we only want to point out the boundaries of relevance of results obtained with models ignoring BH spin.

The post-merger rotational speed of the BH *in*creases monotonically within the three models with initial $a_\mathrm{i} = 0$ spin, from a value of $a_\mathrm{f} = 0.39$ to $a_\mathrm{f} = 0.56$ (see Table 2 and Fig. 9) when *de*creasing the mass ratio and compactness. Following the prescription Eq. (1) an increasing spin decreases both the radius of the horizon and the radius of the ISCO (Fig. 9). In these models the decrease of radius due to spin is larger than the increase due to mass or balances it out, so one observes a slight overall decrease in effective radius (model R5.180) or hardly any change (models R3.160, R2.145): note the lower near-horizontal line in the right panels of Fig. 9.

If at the closest point when the NS material is being accreted by the BH, the radius of the BH remains the same or even shrinks — and with it the effective potential — the effectiveness of matter accretion is reduced. In the end, after tidal disruption, much more material remains in the spiral arc than in the equivalent models without BH spin, e.g. compare R5.180 with M5.180.

The initially rapidly rotating BH (model S2.145) is slowed down from $a_\mathrm{i} = 0.99$ to $a_\mathrm{f} = 0.88$ (Table 2 and Fig. 9). This reduced rotation in itself increases the size of the BH in addition to the increase in mass: note the large increase of the circle outline in the right panels in Fig. 8 and the lower solid line in the bottom right panel of Fig. 9.

Model R3.160 is the only one presented in this paper which shows a distinct orbit widening and repeated mass accretion episodes. In this case the NS remains self-bound, albeit with less mass, after the first close encounter with the BH, and it takes another two episodes before the NS is tidally disrupted. The orbital distance plot (Fig. 9 right panel second from top) looks like the ones from previous works (our work e.g. Janka et al. 1999 and Davies et al. 2005). We return to this point further below.

4. Discussion

We would like to discuss three specific points: (1) the orbit widening during accretion and tidal disruption of the NS, (2) the amount of mass remaining to produce a disk, and (3) the consequences of the NS reaching the ISCO before being tidally disrupted.

4.1. Orbit widening

In previous simulations which used a purely Newtonian potential for the BH, it was noted that during mass accretion from the NS into the BH, the density maximum shifted outwards. This resulted in a lighter NS moving away from the BH on an elliptic orbit. Of course, the shape of the orbit and the gravitational wave emission eventually brought back the NS for a second interaction with the BH, but in the mean time the accretion was effectively shut off. The sequence of mass transfer and orbit widening can be repeated. Numerically this was observed e.g. in Janka et al. (1999; their Fig. 1 shows the orbital separation) and in Rosswog et al. (2004; their Fig. 7 shows the mass accretion episodes). It was explained with a semi-analytic description by Davies et al. (2005), in which some "fraction of the angular momentum of the matter (transferred from the NS to the BH) is fed back into the NS". Their Fig. 1 shows the orbital separation.

Miller (2005) argued that the presence of an ISCO, which is a purely relativistic effect, would substantially alter the outcomes of NS–BH mergers, since the NS would be preferentially absorbed rather than tidally disrupted. This is basically corroborated in the recent general relativistic simulations by Rantsiou et al. (2008), Etienne et al. (2009) and Shibata et al. (2009; their Fig. 1 shows the orbital separation without any sign of orbit widening).

The Paczyński-Wiita potential in our simulations mimics the ISCO, so there is reason to believe the effect as outlined by Miller (2005) is included in our otherwise Newtonian simulations. Indeed, the plots of the distance between the centre of the BH and the centre-of-mass of the NS (Fig. 5, Fig. 9) place our simulations squarely in between the Newtonian and the relativistic results: we observe a beginning of an orbit widening, but it is not long enough to produce a self-bound 'mini'-NS. Especially in the models with large mass ratios and highly compact NSs, the binary distance shrinks down to the 'surface' of the BH and hardly any subsequent orbit widening is seen. The NS is practically absorbed as a whole, as noted in the relativistic calculations.

An exception is model R3.160 (including the potential changing effects of BH spin), which shows the repeated mass accretion episodes very similar to the purely Newtonian models (see Fig. 9 right panel second from top). This might be the consequence of two opposing effects. Firstly, the orbit widening is more pronounced in the models including BH spin (compare right panels of Fig. 9 with the equivalent models in Fig. 5, because the denser regions of the 'escaping' NS are caught up less the smaller BH radius. Secondly, model R3.160 is intermediate between R5.180 where the large BH swallows up the compact NS, and model R2.145 where a small BH produces a large differential tidal field on an extended NS. In this latter case the NS is tidally disrupted although its orbit has widened significantly. The remaining mass in model R3.160 manages to recollect itself into a roughly spherical NS on an elliptic orbit. Recall, however, that this model is a lower-resolution simulation, so the detailed values and sequence of events (e.g. number of cycles) have to be treated with caution.

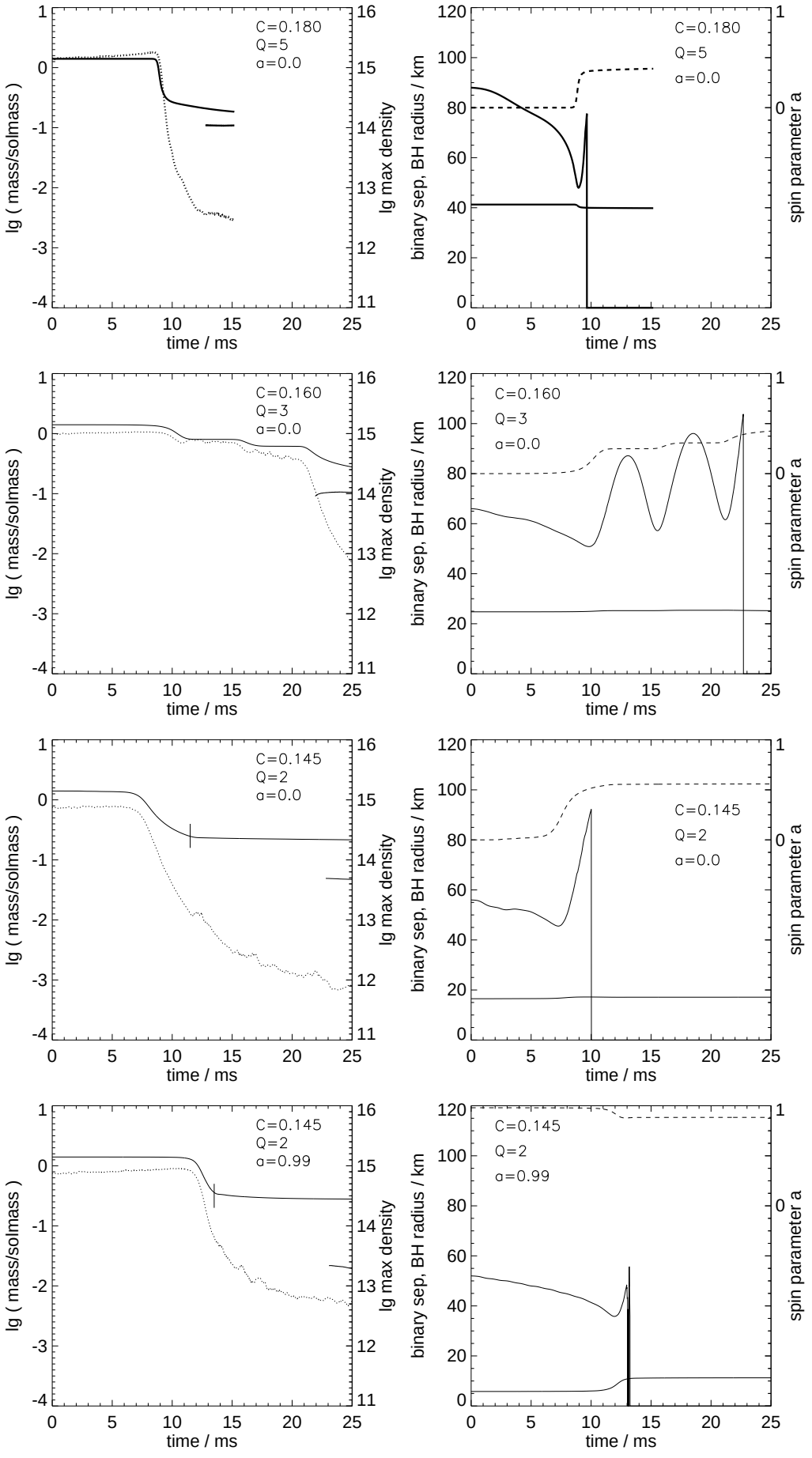

Fig. 9. Temporal evolution for models R2.145, R3.160, R5.180, and S2.145 (from top to bottom), which include the effect of spin-up of the BH (see Table 2). The initial value of the BH rotation parameter is given in the panels. Thin lines show lower-resolution simulations (128^3); bold lines show higher-resolution simulations (256^3). The *left column* of panels shows: the gas mass (solid lines) and the maximum density (dotted lines). A short vertical line indicates the formation of an accretion disk. Short pieces of nearly horizontal lines show the amount of unbound mass. The *right column* of panels shows: the radius of the BH (arithmetic mean of horizon and ISCO) as lower solid line, the binary separation as upper solid line, and the BH spin parameter a as top dashed line. The vertical line indicates when the mass within a sphere around the density maximum falls below 0.03 $M_\odot$.

Table 2. Key initial model parameters and some results for models including BH spin. Initial parameters: mass ratio Q, compactness C, black hole mass $M_{\rm BH}$, initial BH spin parameter $a_{\rm i}$, neutron star radius $R_{\rm NS}$, initial orbital distance $d_{\rm i}$, number of zones per dimension N, size of largest grid L, size of finest zone $\Delta x = L/8N$. The mass of the NS is 1.4 $M_\odot$ in all cases. Values at the end of the simulation: unbound+ejected gas mass $M_{\rm u}$, bound neutron star mass around BH $M_{\rm b}$, neutron star mass not instantly accreted by BH $M_{\rm g}$, final BH spin parameter $a_{\rm f}$.

Model	Q	C	$M_{\rm BH}$	$a_{\rm i}$	$R_{\rm NS}$	$d_{\rm i}$	N	L	Δx	$M_{\rm u}$	$M_{\rm b}$	$M_{\rm g}$	$a_{\rm f}$
			$M_\odot$		km	km		km	km	$M_\odot$	$M_\odot$	$M_\odot$	km
R5.180	5	0.180	7.0	0.00	11.5	88	256	1450	0.71	0.11	0.07	0.18	0.39
R3.160	3	0.160	4.2	0.00	14.3	66	128	1100	1.07	0.11	0.17	0.28	0.43
R2.145	2	0.145	2.8	0.00	14.3	56	128	880	0.86	0.05	0.17	0.22	0.56
S2.145	2	0.145	2.8	0.99	14.3	52	128	850	0.83	0.02	0.26	0.28	0.88

4.2. Disk Mass

The amount of material not 'instantly' absorbed by the BH but remaining in the surroundings and potentially available to form a torus, is important as energy source to power the jet of a gamma-ray burst. Thus the questions of how much matter gets accreted, how much gets ejected, and how much forms a torus, need to be investigated carefully. In this point, the recent numerical general relativistic simulations (Rantsiou et al. 2008; Etienne et al. 2009; Shibata et al. 2009, their Fig. 7) still differ markedly between themselves, even for models with similar parameters. The range spans from $\approx 0.1\,M_\odot$ to less than $10^{-4}\,M_\odot$. To power gamma-ray bursts effectively, at least some hundredths of a solar mass seem to be needed.

The values of mass remaining around the BH for our models are tabulated in Tables 1 and 2. Only in models with a compact NS ($C = 0.180$) and only for non-rotating BHs, does most of the matter get accreted quickly by the BH and only 10^{-2}–$10^{-3}\,M_\odot$ remain to form a torus, especially for the massive BHs with large mass ratio Q. This trend matches the general relativistic findings; however, the absolute quantities of mass are larger in our models, e.g. Shibata et al. (2009) obtain typically 1% of the neutron star mass for models with small mass ratio Q. On the other hand, Etienne et al. (2009) get $0.06\,M_\odot$ for a non-rotating BH model with $Q = 3$. For less compact NSs, we obtain around $0.1\,M_\odot$.

All our models including the effect of BH spin (Table 2) end with a significant amount (between $0.18\,M_\odot$ and $0.28\,M_\odot$ of NS material spread out around the BH, due to following effect: the BH's effective potential depth shrinks because the spin-up matches or outweighs the mass increase (Fig. 9, models R5.180, R2.145). This reasoning has been expounded further above.

4.3. Tidal disruption vs. ISCO

Following Miller's (2005) argument, we would expect little mass (tenth of a percent of a solar mass, or less) to remain around the BH if the NS reaches the ISCO before being tidally shredded. On the other hand, if the NS is tidally disrupted ('mass shedding', MS) before reaching the ISCO, then significant amounts of matter (several percent of a solar mass) would be able to form a torus around the BH. With this in mind, and to be able to compare to previous relativistic simulations, we chose the model parameters as plotted in Fig. 2. This graph also uses different symbols to show the varying remaining gas mass around the BH. No clear correlation pattern can be seen between the remaining gas mass and the expected line separating the ISCO from the MS case, except a general trend that the mass is indeed smaller toward the right (models with higher compactness). However, we cannot identify a clear step change. This lack of clear demarcation between ISCO and MS is also the case for the models including general relativity (Shibata et al. 2009, Fig. 3).

One point to remember is that the mass ratio Q and compactness C used in this paper, are based on the purely Newtonian, uniquely defined, masses of NS and BH, and radius of the NS. Of course, in the models with general relativistic physics, Q and C have to be defined with a specific choice of ADM mass, rest mass, circumferential radius, isotropic radius, etc. This makes the comparison between our Newtonian results shown in Fig. 2 and the general relativistic work by others in Fig. 3 not straightforward. We would expect that these differences produce a shift of the separating line within the plot, but guess it would be by only several tens of percent, and therefor not qualitatively change the statements.

4.4. Rotating BH

For models R5.180, R3.160, R2.145, and S2.145 we only want to note that a large difference is present to the equivalent non-rotating polytropic models (for details see Sect. 3.3 and end of Sects. 4.1 and 4.2). It is outside the scope of this paper to map out the differences in detail over the full parameter space. It will be the topic of a subsequent investigation. We note that Etienne et al. (2009) report a fairly large torus mass ($0.2\,M_\odot$) in their $Q = 3$ model with a spinning BH ($a = 0.75$).

Our values for the final spin parameter of the BH (0.39, 0.43, 0.56) match the values obtained by Shibata et al. (2009; their Table III) fairly well, although their values are systematically larger (0.42, 0.56, 0.68, respectively).

In our pseudo-Newtonian simulations, the mass that assembles into a torus or gets ejected, shows a very strong sensitivity to the inclusion of the angular momentum gain by the BH due to the accretion of matter in the merger. This effect, however, should be generically included in the relativistic models of Shibata et al. (2009) and Etienne et al. (2009).

Since the existence of an ISCO is accounted for by the BH potentials used in our simulations, the tendency to larger torus and ejecta masses found in our models compared to relativistic simulations (with similar system parameters) requires a different explanation. We hypothesize that the difference could be a consequence of the stronger self-gravity of relativistically described neutron stars in contrast to the Newtonian objects considered in our simulations. The deeper relativistic potential might impede the disruption of the neutron star and the formation of a tidal arc, so that a bigger fraction of the star is directly swallowed by the BH.

5. Conclusions

1. We do not note a fundamental and discontinuous difference in the dynamics of the models in the ISCO regime as opposed to the 'mass shedding' (= tidal disruption) regime. The variation of masses that are not instantly accreted by the BH is continuous (Figs. 2 and 3).
2. In all cases the NS is tidally stretched into an arc, albeit with very different masses for the various cases.
3. For models without BH spin the onset of orbit widening is noted during the phase of tidal shredding of the NS, but it is only short lived.
4. In one case of a model including the BH spin we see the formation of a 'mini' NS on an extended elliptic orbit, followed by episodic mass transfer, and a final tidal disruption.
5. In mergers with compact neutron stars ($C = 0.180$) a very small amount, less than $10^{-2} M_\odot$, remains in the surroundings of the BH.
6. Only in mergers with small BHs, mass ratio $Q = 2$ or $Q = 3$, does an accretion torus get formed.
7. Mergers with neutron stars of compactness $C = 0.145$ or $C = 0.160$ yield a significant amount of material (around $0.1 M_\odot$) around the BH.
8. Effects due to BH spin-up are essential and significantly change the results. We note an increase in mass in the material surrounding the BH up to 0.2–0.3 $M_\odot$.

Acknowledgements. MR would like to thank the Max-Planck-Institut für Astrophysik for the kind hospitality during a sabbatical visit, where this work was accomplished. We thank A. Bauswein for stimulating and helpful discussions. The calculations were performed at the Rechenzentrum Garching (RZG). The project was also supported by the Deutsche Forschungsgemeinschaft through the Transregional Collaborative Research Centers SFB/TR 27 "Neutrinos and Beyond" and SFB/TR 7 "Gravitational Wave Astronomy", and the Cluster of Excellence EXC 153 (`http://www.universe-cluster.de`) "Origin and Structure of the Universe".

References

Abramowicz, M.A., 2009, arXiv:0904.0913
Artemova, I.V., Björnsson, G. & Novikov, I.D. 1996, ApJ, 461, 565
Colella, P. & Woodward, P.R. 1984, J. Comput.Phys., 54, 174
Davies, M.B., Levan, A.J. & King, A.R. 2005, MNRAS, 356, 54
Etienne, Z.B., Faber, J.A., Liu, Y.T., Shapiro, S.L., Taniguchi, K. & Baumgarte, T.W. 2008, Phys. Rev. D, 77, 084002
Etienne, Z.B., Liu, Y.T., Shapiro, S.L. & Baumgarte, T.W. 2009, Phys. Rev. D, 79, 044024
Janka, H.-Th., Eberl, T., Ruffert, M., & Fryer C.L. 1999, ApJ, 527, L39
Lee, W.H., Ramirez-Ruiz, E. & Granot, J. 2005, ApJL, 630, L165
Miller, M.C. 2005, ApJ, 626, L41
Oechslin, R. & Janka, H.-Th. 2006, 368, 1489
Paczyński, B. & Wiita, P. 1980, A&A, 88, 32
Portegies Zwart, S.F. 1998, ApJ, 503, L53
Rantsiou, E., Kobayashi, S., Laguna, P. & Rasio, F.A. 2008, A&A, 680, 1326
Rasio, F.A. & Shapiro, S.L. 1999, Class. Quant. Grav., 16, R1
Rosswog, S., Speith, R. & Wynn, G.A. 2004, MNRAS, 351, 1121
Ruffert, M. 1992, A&A, 265, 82
Ruffert, M. & Janka, H.-Th. 2001, A&A, 380, 544
Ruffert, M., Janka, H.-Th. & Schaefer, G. 1996, A&A, 311, 532
Ruffert, M., Janka, H.-Th., Takahashi, K. & Schaefer, G. 1997, A&A, 319, 122
Setiawan, S., Ruffert, M. & Janka, H.-Th. 2006, A&A, 458, 553
Shen, H., Toki, H., Oyamatsu, K. & Sumiyoshi, K., 1998, Nucl. Phys. A, 637, 435
Shibata, M., Kyutoku, K., Yamamoto, T. & Taniguchi, K. 2009, Phys. Rev. D, 79, 044030
Taniguchi, K., Baumgarte, T.W., Faber, J.A. & Shapiro, S.L. 2008, Phys. Rev. D, 77, 044033